Journal of Luminescence 243 (2022) 118675

Contents lists available at ScienceDirect

Journal of Luminescence

journal homepage: www.elsevier.com/locate/jlumin

Tailoring Bi_2MoO_6 by Eu^{3+} incorporation for enhanced photoluminescence emissions

Ivo M. Pinatti [a,b,*], Fabio A. Pires [c], Priscila B. Almeida [c], Paula F.S. Pereira [c], Marcio D. Teodoro [d], E. Guillamón [b], Alexandre Z. Simões [a], Juan Andrés [b,**], Elson Longo [c], Ieda L.V. Rosa [c]

[a] Faculty of Engineering of Guaratinguetá, São Paulo State University (UNESP), 12516-410, Guaratinguetá, SP, Brazil
[b] Department of Analytical and Physical Chemistry, University Jaume I (UJI), Castelló, 12071, Spain
[c] CDMF, LIEC, Federal University of São Carlos, P.O. Box 676, São Carlos, 13565-905, Brazil
[d] Physics Department, Federal University of São Carlos, P.O. Box 676, São Carlos, 13565-905, Brazil

ARTICLE INFO

Keywords:
Bi2MoO6
Eu3+
Microwave-assisted solvothermal
Photoluminescence

ABSTRACT

Here, an experimental study is presented on the structural, electronic, and optical properties of $Bi_{2-x}MoO_6$:xEu^{3+} (x = 0, 0.5, 1.0, 2.0, and 4.0 mol%) materials, synthesized by means of the microwave-assisted solvothermal method using ethylene glycol as a solvent. Different characterization techniques (X-ray diffraction measurements with Rietveld refinements, Raman and ultraviolet–visible diffuse reflectance spectroscopy, field emission scanning electron microscopy, and photoluminescence emissions) have been employed to examine the structural and electronic properties, energy transfer and defect evolution which control the performance of the as-synthetized materials. Present findings provide deep insights into the substitution of Eu^{3+} cations in Bi_2MoO_6, with focus on their influence on process that dictate the superior optical properties.

1. Introduction

The emergence of precise and scalable synthetic methods for producing new photoluminescent (PL) materials provides opportunities to tune photophysical properties beyond their band gaps, and to incorporate them in optical devices. The substitution of rare-earth (RE^{3+}) cations, acting as activators, in inorganic compounds, is capable to change the local structures towards the modulation of their electrical and optical properties, and playing a crucial role in light-emitting materials [1–5]. Moreover, these materials have attracted considerable attention for applications in different fields such as optical amplifiers, biomedical diagnostics, and optical bioprobes [6–10]. In particular, the PL spectra are associated with the abundant 4f orbitals electron configuration, displaying mainly 4f–4f, 4f–5d, and charge transfer transitions, which results in narrow emission lines, high photostability, and an intense luminescence from ultraviolet (UV) to near-infrared [11]. Among RE^{3+} cations, europium (Eu^{3+}) is the most promising for this purpose and it exhibits intense PL red emission due to $^5D_0 \rightarrow {}^7F_2$ transition around 615 nm [12–14]. Examples of Eu^{3+} cations substitution in different kinds of materials like glasses, organic compounds, polymers, inorganic matrix, among others, are extensively reported [15–24].

Bismuth oxides of formula $(Bi_2O_2)^{2+}(A_{n-1}B_nO_{3n+1})^{2-}$ (A = Ca, Sr, Ba, Pb, Bi, Na, K, and B = Ti, Nb, Ta, Mo, W, Fe) are interesting materials due to their layered structure composed of perovskite slabs of $(A_{n-1}BnO_{3n+1})^{2-}$ between $(Bi_2O_2)^{2+}$ layers. One representative example of this family is the bismuth molybdate, Bi_2MoO_6 (BMO), due to its versatile applications, including gas sensing [25], electrical [26–31] and photocatalytic [32–56] properties. A wide variety of synthesis methods have been employed to obtain BMO, such as co-precipitation and spray-drying [55], sol-gel [57], mechanochemical [34], sonochemical [58], solid-state [38,50,59], hydrothermal [25,32,33,45,47,49,51,52,60–66], polymeric precursor [67], and citric acid complex process [68], among others [69].

The structure, PL and photocatalytic properties of a wide range of BMO materials with presence of RE^{3+} cations were studied in depth [59–64,67,68,70–74]. However, these materials were obtained by expensive and long-lasting methods and most of the time presented low PL emissions. In previous studies, our research group has successfully

* Corresponding author. Faculty of Engineering of Guaratinguetá, São Paulo State University (UNESP), 12516-410, Guaratinguetá, SP, Brazil.
** Corresponding author.
E-mail addresses: ivo.m.pinatti@unesp.br (I.M. Pinatti), andres@qfa.uji.es (J. Andrés).

https://doi.org/10.1016/j.jlumin.2021.118675
Received 6 July 2021; Received in revised form 11 November 2021; Accepted 9 December 2021
Available online 10 December 2021

obtained Eu^{3+} substitution in different materials such as α-Ag_2WO_4 [5, 75–77], ZrO_2 [78,79], $CaMoO_4$ [80], $ZnMoO_4$ [81], and $CaZrO_3$. [82] Additionally, Eu^{3+} cations substituted in BMO material was only obtained by conventional hydrothermal [61,63,64,83,84], sol-gel [85], solid-state [59,72,86–88], and citric acid complex [68] methods so far. Therefore, environmentally friendly synthetic procedure of these materials with outstanding optical efficiency is still challenging.

For the successful manufacturing of such materials, the structure, distribution, and electronic properties of the RE^{3+} cations on the host lattice must be known. To the best of our knowledge, the characterization and studies of optical properties of the as-synthetized $Bi_{2-x}MoO_6$: xEu^{3+} (BMOxEu) samples by the microwave-assisted solvothermal (MAS) method are lacking. This study systematically investigated the effect of the addition of different amounts of Eu^{3+} cations into the BMO host lattice on the structural, electronic and optical properties. These samples were obtained by the MAS method using low temperature and short reaction time, and the samples were denoted as BMO, BMO0.5Eu, BMO1Eu, BMO2Eu, and BMO4Eu, corresponding to the pure-Bi_2MoO_6, 0.5, 1.0, 2.0, and 4.0 mol% Eu^{3+} samples, respectively.

2. Results and discussion

The BMOxEu materials were efficiently synthesized by the MAS method at 160 °C for 32 min. X-ray diffraction (XRD) patterns of the BMOxEu crystals, illustrated in Fig. 1A, showed narrow and sharp peaks indicating a high degree of crystallinity in all cases and are in good agreement with an orthorhombic structure with *Pca2₁* space group according to the inorganic crystal structure database, *ICSD* 20–1685 [89]. Thus, no impurities were detected and the percentage of Eu3+ cations was not sufficient to form secondary phases. Fig. SI-1 (a-e) shows the Rietveld refinement plot of observed *versus* calculated pattern of the BMOxEu crystals. The difference between XRD profiles for experimentally observed and theoretically calculated was at near zero in the intensity scale, as shown by the line (Y_{Obs} - Y_{Calc}). Tables SI–1 shows the experimental lattice parameters and details on the quality of the structural refinement. Small deviations of the statistical parameters (R_w and GOF) were observed, attesting the reliability and accuracy of the refinement results.

Fig. 1B shows the unit cell representation of the BMO1Eu structure simulated through the visualization for electronic and structural analysis (VESTA) program [90,91] using the lattice parameters and atomic positions listed in Tables SI–1. The BMO1Eu unit cell observed is constituted of two types of Bi octahedral clusters, namely [$Bi(1)O_6$] and [$Bi(2)O_6$], and one type of Mo octahedral cluster, namely [MoO_6]. The Bi^{3+}-by-Eu^{3+} substitution is attested by the percentage of the ion radius between the host ion and the doped ion, which usually is less than 30%. Considering Bi^{3+} (CN = 6, IR = 1.03 Å), Mo^{6+} (CN = 6, IR = 0.59 Å), and Eu^{3+} (CN = 6, IR = 0.947 Å) cations [92], the calculated percentages of Bi^{3+} and Mo^{6+} are 8.05% and −60.5%, respectively. As a consequence, the refinement results show that the Eu^{3+} cations may occupy either [$Bi(1)O_6$] or [$Bi(2)O_6$] clusters in the BMO lattice [93]. Also, a percentage of Eu^{3+} cations can also be presented in the interstitial sites of the host lattice, as the lattice parameters do not change systematically. It happens because Eu^{3+} cations are treated as impurities into the host lattice which dramatically decrease the organization of the $(MoO_4)^{2-}$ and $(Bi_2O_2)^{2+}$ layers within the crystal lattice, promoting the formation of structural defects (oxygen vacancies, distortion of bonds, stresses, strains, etc.). These results are similar to those observed for other RE^{3+} substituted BMO materials in which refinement results show a mean of the overall values of substitution, not necessarily indicating the precise location of Eu^{3+} cations [67,71,72].

Fig. 1C presents the obtained Raman spectra for BMOxEu crystals synthesized by the MAS method. The increasing concentration of Eu^{3+} cations in the crystalline network has a marked effect on the intensity of all vibrational modes, indicating that the substitution of Bi^{3+} cations causes changes in the chemical environment capable of promoting octahedral distortions, reducing symmetry and, consequently, decreasing the structural order at a short-range. In particular, the band at 800 cm^{-1} which corresponds to the stretching mode of the Mo–O bond in the octahedral [MoO_6] cluster, can be considered as a signature

Table 1
FWHM of 800 cm^{-1} Raman band, E_{gap}, and CIE chromatic coordinates of emission spectra of BMOxEu crystals.

$Bi_{2-x}MoO_6$: xEu^{3+}	Raman FWHM	E_{gap} (eV)	Chromatic coordinate			
			λ_{exc} = 355 nm		λ_{exc} = 290 nm	
			x	y	x	y
x = 0	29.01	3.03	0.299	0.263	0.548	0.424
x = 0.5	31.10	3.05	0.230	0.214	0.560	0.415
x = 1	33.28	3.15	0.280	0.297	0.562	0.414
x = 2	34.16	3.14	0.226	0.225	0.549	0.424
x = 4	42.40	3.31	0.281	0.270	0.547	0.426

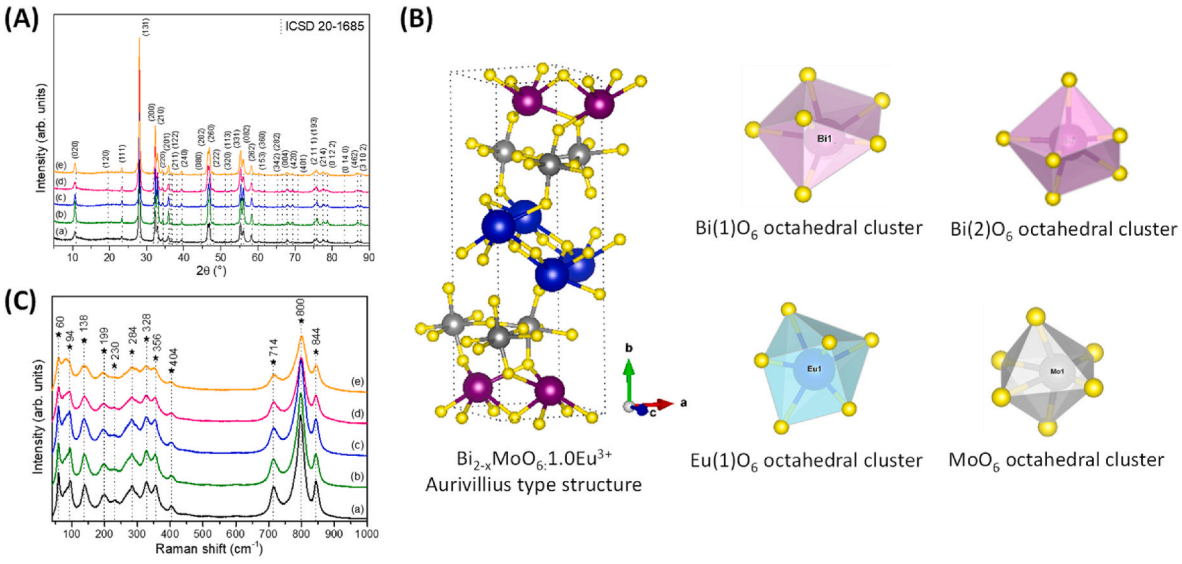

Fig. 1. (A) XRD patterns, (B) Schematic representation of the unit cell of BMO1Eu, and (C) Raman spectra of (a) BMO, (b) BMO0.5Eu, (c) BMO1Eu, (d) BMO2Eu, and (e) BMO4Eu crystals.

of the structural change of the BMO lattice provoked by the inclusion of Eu^{3+} cations. Table 1 presents the values of the full width at half maximum (FWHM) for the mode at 800 cm^{-1}. An analysis of the results renders an increment of the FWHM values as the Eu^{3+} concentration increases, as well as appreciable decrease of the intensity for this band. In addition, we can also sense a general broadening of all vibrational modes as the amount of Eu^{3+} cations increases, and it is also reported in previously studies devoted to the substitution of RE^{3+} cations in the BMO [61,71].

Fig. SI-2(A) shows the UV–vis diffuse reflectance spectra for the BMOxEu crystals, which showed absorption in the visible range of approximately 450 nm for all crystals. Fig. SI-2(B) shows the graphs obtained by the Kubelka & Munk-Aussig method for BMOxEu crystals and the E_{gap} values obtained are listed in Table 1. It was observed a small increase on the E_{gap} values as the Eu^{3+} concentration increases. Besides the limitation of the equipment and the band gap estimation due to the small percentage of Eu^{3+} cations, the increase on the values can also be attributed to the presence of structural defects, and different acceptor species in the valence band (VB) region associated with donator species in the conduction band (CB) region. Specifically, for the BMOxEu crystals, the variation in the band gap values may be due to Eu^{3+} 4f orbitals which are responsible for generating separation between VB and CB as cited in other published works [61,62,67,71,93].

Photoluminescence (PL) measurements were performed by two distinct equipment. Firstly, Fig. 2 shows the PL emission spectra of the BMOxEu crystals under laser excitation at a wavelength of 355 nm. PL emission band of semiconductor materials are mainly originated by the recombination of photo-generated electron-hole pairs [94]. Particularly, the PL emission band at 445 nm is due recombination of these pairs within the [MoO_6] clusters. Moreover, for BMOxEu crystals, Eu^{3+} cations are responsible for increasing the structural and electronic defects due to [EuO_6] clusters, contributing to the broadening and different intensity of this band. These results indicate that the PL behavior arises from intrinsic defects of the host lattice, and extrinsic defects due to Eu^{3+} cations [59]. Additionally, for BMOxEu crystals, a narrow and well-defined peak characteristic of the Eu^{3+} cations at 615 nm was observed, related to the $^5D_0 \rightarrow {}^7F_2$ transition. Finally, plate/flake-like morphologies tend to have the largest specific surface area and the strongest light absorption, which contributed to the results observed [61].

Secondly, PL excitation and PL emission spectra were performed on a Xe lamp source equipment. Fig. 3A shows the PL excitation spectra of BMOxEu crystals monitoring the emission wavelength at 615 nm, which represents the Eu^{3+} cations maximum PL emission ascribed to the $^5D_0 \rightarrow {}^7F_2$ transition. A broad band in the range of 250–375 nm is

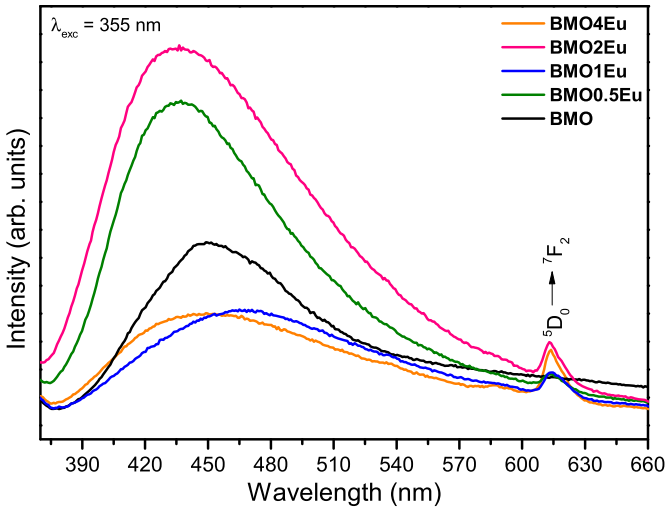

Fig. 2. PL emission spectra of the BMOxEu crystals excited by a 355 nm laser.

observed for all samples which is characteristic of mixed and indistinguishable: i) ligand-to-metal charge transfer (LMCT) state of $O^{2-} \rightarrow Mo^{6+}$ of the [MoO_6] clusters and ii) charge transfer band (CTB) of $O^{2-} \rightarrow Eu^{3+}$ [72,93]. A peak located at 394 nm was also observed, which is related to the $^7F_0 \rightarrow {}^5L_6$ transition of Eu^{3+} cations [75,76]. Fig. 3B shows the PL emission spectra for BMOxEu crystals when excited at 290 nm, maximum intense of the absorption band observed in the PL excitation spectra. Analyzing Fig. 3B, well-defined peaks can be ascribed to the f-f transitions of the Eu^{3+} cations which are located at 592 ($^5D_0 \rightarrow {}^7F_1$), 615 ($^5D_0 \rightarrow {}^7F_2$), and 695 nm ($^5D_0 \rightarrow {}^7F_4$). These results illustrate that Eu^{3+} cations with low 4f → 4f absorption efficiency in the NUV region can be an activator of the red emitting phosphor and be excited by UV LEDs. Therefore, BMO matrix acts as an efficient host activator for the Eu^{3+} cations due to the energy transfer from the [MoO_6] to the [EuO_6] clusters.

Comparing the samples, BMO1Eu present the highest PL intensity, ascribing 1.0 mol% Eu^{3+} cations as the quenching concentration for this matrix. Moreover, Eu^{3+} cations can be used as a site environmental probe due to the relative ratio of the $^5D_0 \rightarrow {}^7F_1$ (magnetic dipole) and $^5D_0 \rightarrow {}^7F_2$ (electric dipole) transitions. It is clearly seen that the $^5D_0 \rightarrow {}^7F_2$ transition is more intense than the $^5D_0 \rightarrow {}^7F_1$ one, indicating that Eu^{3+} cations are located predominantly in a site without inversion of symmetry [63,95]. Fig. 3C shows a schematic energy level diagram and a proposed energy transfer mechanism under 290 nm excitation for the BMOxEu crystals. It is observed that under excitation at 290 nm, electrons are excited from valence band (VB) into the charge transfer state (CTS) of the [MoO_6] clusters. Then, the excitation energy is transferred from the [MoO_6] clusters to the $^5D_4$ level of Eu^{3+} cations. Finally, Eu^{3+} cations in the populated $^5D_4$ level undergo multiphonon relaxation to the luminescent $^5D_0$ level that radiatively relax to ^7F_J (J = 1, 2, and 4) levels, resulting in the characteristic PL emissions of Eu^{3+} cations.

Measurement of color that the human eye perceives was evaluated by the *Commission internationale de l'éclairage* (CIE) chromaticity diagram. Fig. 4 shows the CIE diagram for the samples excited at 355 nm (Figs. 4A) and 290 nm (Fig. 4B), and the calculated values for the x and y coordinates are listed in Table 1. When the crystals are excited by 355 nm laser, blue region color is observed due to the predominant intense PL emission within [MoO_6] clusters, whereas at 290 nm excitation, orange-red color intense PL emission is observed because of higher Eu^{3+} f-f transitions contribution. For BMO1Eu crystal, the values for the x and y coordinates are close to those published for the chromaticity coordinates of the international standards of commercial phosphorus. This result point out that 1.0 mol% Eu^{3+} is the best concentration for phosphor application in the red emitting region of electromagnetic spectrum [77].

Field emission scanning electron microscopy (FE-SEM) images of BMOxEu crystals are shown in Fig. 5. The images confirm the *flake-like* morphology and smooth surfaces of the crystals, as similarly reported by Y. Zhu et al. and L. Xie et al. [46,53,69,96] BMO0.5, BMO1Eu, and BMO2Eu crystals show little variation in the organization patterns of the platelets, as well as in the width and length of the crystallites. For the BMO4Eu crystal, a decrease in the lateral dimensions of the crystallites is observed, while maintaining homogeneous thickness with values in the 15–45 nm range. Considering the Ostwald ripening model for crystal growth, it can be affirmed that the excess defect constituted by the addition of a high concentration of Eu^{3+} cations created a larger number of crystallite germination centers, therefore reducing the size of each one [53,61,62].

3. Conclusions

$Bi_{2-x}MoO_6$:xEu^{3+} (x = 0, 0.5, 1.0, 2.0, and 4.0 mol%) materials were prepared via MAS method using ethylene glycol as a solvent. The orthorhombic structure was confirmed by XRD patterns without the presence of secondary phases, whereas the results for the Raman spectroscopy confirm structural short-range disorder as shown by the

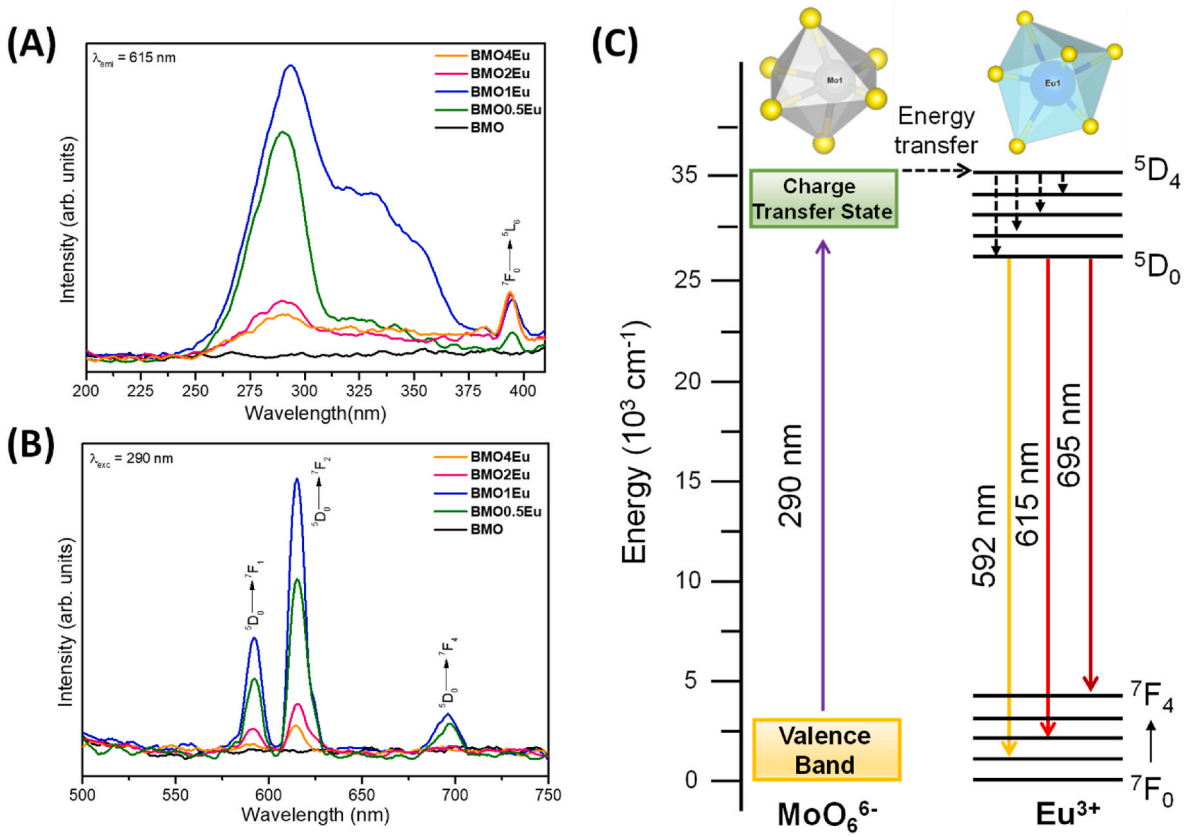

Fig. 3. (A) PL excitation spectra of the BMOxEu crystals monitoring emission at 615 nm, (B) PL emission spectra of the BMOxEu crystals excited at 290 nm, and (C) Schematic energy level diagram and a proposed energy transfer mechanism for the BMOxEu crystals.

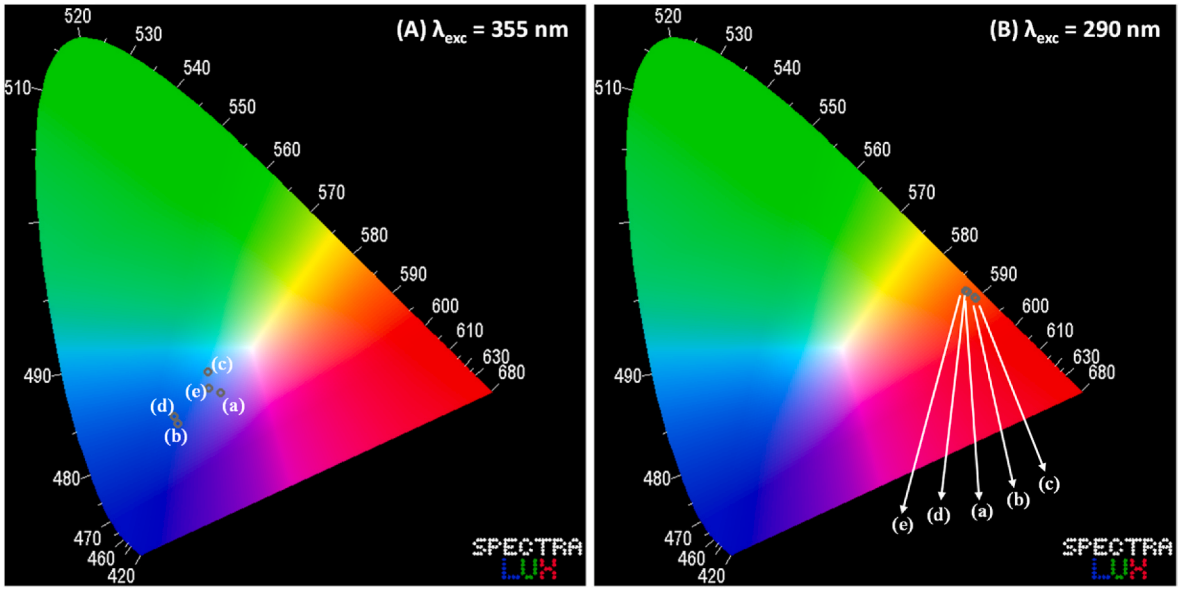

Fig. 4. CIE chromatic diagram of the PL emission spectra of BMOxEu crystals excited at (A) 355 nm, and (B) 290 nm. (a) BMO, (b) BMO0.5Eu, (c) BMO1Eu, (d) BMO2Eu, and (e) BMO4Eu.

enlargement of the vibrational modes. UV–vis spectroscopy results render that the substitution of Eu^{3+} cations favors the increase of the value of the direct band gap. The intensity of the PL emission intensity is enhanced as the Eu^{3+} concentration increases, and the optimal concentration is 1.0 mol% Eu^{3+} cations. In addition, it is quite clear that PL and photocatalysis in a semiconductor are closely related; in future projects will study the substitution of Eu^{3+} cations in Bi_2MoO_6 as a promising strategy to investigate photocatalytic applications.

Credit author statement

Authors I.M.P, F.A.P, P.B.A., P.F.S.P, M.D.T., E.G., A.Z.S., J.A., E.L.,

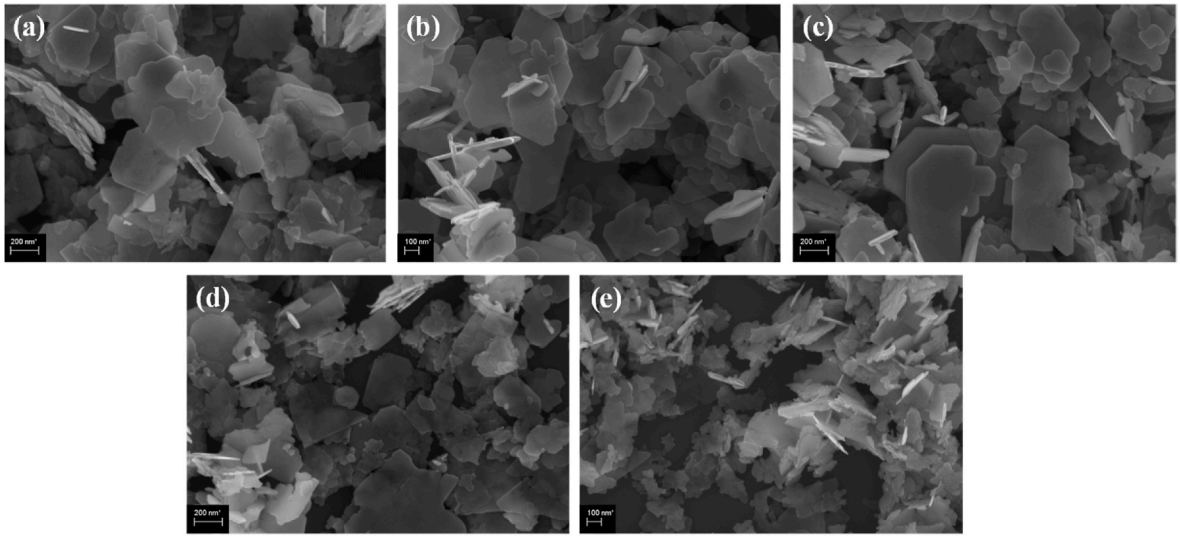

Fig. 5. FE-SEM images of (a) BMO, (b) BMO0.5Eu, (c) BMO1Eu, (d) BMO2Eu, and (e) BMO4Eu crystals.

and I.L.V.R., contributed equally to perform the required experiments, analyse the data and write the paper. All authors reviewed the manuscript.

Declaration of competing interest

The authors declare that they have no known competing financial interests or personal relationships that could have appeared to influence the work reported in this paper.

Acknowledgments

The authors are grateful for the support of the Brazilian research financing institution Fundação de Amparo à Pesquisa do Estado de São Paulo (FAPESP; Grant Nos. 13/07296-2, 18/09530-6, 19/03722-3, and 19/25944-8). They also wish to thank Rorivaldo Camargo (CDMF-UFSCar), Sandra Maria Terenzi Bellini (CDMF-UFSCar), Prof. Osvaldo Antonio Serra (FFCLRP-USP), and Ayla Roberta Borges da Silva Galaço (FFCLRP-USP) for technical and scientific contributions. J.A., and E.G. acknowledge Universitat Jaume I (project UJI-B2019-30) and the Ministerio de Ciencia, Innovación y Universidades (Spain) (project PGC2018094417-B-I00).

Appendix A. Supplementary data

Supplementary data to this article can be found online at https://doi.org/10.1016/j.jlumin.2021.118675.

References

[1] T. Jüstel, H. Nikol, C. Ronda, New developments in the field of luminescent materials for lighting and displays, Angew. Chem. Int. Ed. 37 (1998) 3084–3103, https://doi.org/10.1002/(SICI)1521-3773(19981204)37:22<3084::AID-ANIE3084>3.0.CO;2-W.

[2] B. Shao, J. Huo, H. You, Prevailing strategies to tune emission color of lanthanide-activated phosphors for WLED applications, Adv. Opt. Mater. 7 (2019) 1–23, https://doi.org/10.1002/adom.201900319.

[3] M. Shang, C. Li, J. Lin, How to produce white light in a single-phase host? Chem. Soc. Rev. 43 (2014) 1372–1386, https://doi.org/10.1039/c3cs60314h.

[4] N. Jain, R. Paroha, R.K. Singh, S.K. Mishra, S.K. Chaurasiya, R.A. Singh, J. Singh, Synthesis and rational design of europium and lithium doped sodium zinc molybdate with red emission for optical imaging, Sci. Rep. 9 (2019) 1–14, https://doi.org/10.1038/s41598-019-38787-1.

[5] I.M. Pinatti, P.F.S. Pereira, M. de Assis, E. Longo, I.L.V. Rosa, Rare earth doped silver tungstate for photoluminescent applications, J. Alloys Compd. 771 (2019) 433–447, https://doi.org/10.1016/j.jallcom.2018.08.302.

[6] S.K. Ray, Y.K. Kshetri, S.W. Lee, Upconversion luminescence properties of BaMoO4:Yb3+, Ln3+ (Ln3+=Er3+/Tm3+, Er3+/Tm3+/Ho3+) micro-octahedrons, Nanotechnology 30 (2019) 454002, https://doi.org/10.1088/1361-6528/ab37ac.

[7] D. Li, W. Wang, X. Liu, C. Jiang, J. Qiu, Discovery of non-reversible thermally enhanced upconversion luminescence behavior in rare-earth doped nanoparticles, J. Mater. Chem. C. 7 (2019) 4336–4343, https://doi.org/10.1039/c9tc01009b.

[8] F. Wang, Y. Han, C.S. Lim, Y. Lu, J. Wang, J. Xu, H. Chen, C. Zhang, M. Hong, X. Liu, Simultaneous phase and size control of upconversion nanocrystals through lanthanide doping, Nature 463 (2010) 1061–1065, https://doi.org/10.1038/nature08777.

[9] H. Dong, L.D. Sun, C.H. Yan, Energy transfer in lanthanide upconversion studies for extended optical applications, Chem. Soc. Rev. 44 (2015) 1608–1634, https://doi.org/10.1039/c4cs00188e.

[10] X. Zhou, J. Qiao, Z. Xia, Learning from mineral structures toward new luminescence materials for light-emitting diode applications, Chem. Mater. (2021), https://doi.org/10.1021/acs.chemmater.1c00032.

[11] G.B. Nair, H.C. Swart, S.J. Dhoble, A review on the advancements in phosphor-converted light emitting diodes (pc-LEDs): phosphor synthesis, device fabrication and characterization, Prog. Mater. Sci. 109 (2020) 100622, https://doi.org/10.1016/j.pmatsci.2019.100622.

[12] M. Toro-González, R. Copping, S. Mirzadeh, J.V. Rojas, Multifunctional GdVO4:Eu core-shell nanoparticles containing 225Ac for targeted alpha therapy and molecular imaging, J. Mater. Chem. B. 6 (2018) 7985–7997, https://doi.org/10.1039/c8tb02173b.

[13] H. Kaur, M. Jayasimhadri, Color tunable photoluminescence properties in Eu3+ doped calcium bismuth vanadate phosphors for luminescent devices, Ceram. Int. 45 (2019) 15385–15393, https://doi.org/10.1016/j.ceramint.2019.05.034.

[14] N. Zhang, J. Li, J. Wang, R. Shi, L. Chen, A. Zhang, P. Yang, A vanadate-based white light emitting luminescent material for temperature sensing, RSC Adv. 9 (2019) 30045–30051, https://doi.org/10.1039/c9ra06193b.

[15] A. Jose, P. Remya Mohan, T. Krishnapriya, T.A. Jose, A.C. Saritha, N. V. Unnikrishnan, C. Joseph, P.R. Biju, Phonon sideband and Judd–Ofelt analyses of trivalent europium doped fluoroborosilicate glasses for red emitting device applications, J. Mater. Sci. Mater. Electron. 31 (2020) 13531–13540, https://doi.org/10.1007/s10854-020-03909-3.

[16] Y. Kitagawa, S. Wada, M.D.J. Islam, K. Saita, M. Gon, K. Fushimi, K. Tanaka, S. Maeda, Y. Hasegawa, Chiral lanthanide lumino-glass for a circularly polarized light security device, Commun. Chem. 3 (2020) 1–5, https://doi.org/10.1038/s42004-020-00366-1.

[17] M.M. Yawalkar, G.B. Nair, G.D. Zade, S.J. Dhoble, Effect of the synthesis route on the luminescence properties of Eu3+ activated Li6M(BO3)3 (M = Y, Gd) phosphors, Mater. Chem. Phys. 189 (2017) 136–145, https://doi.org/10.1016/j.matchemphys.2016.12.006.

[18] G.B. Nair, S.J. Dhoble, Photoluminescence properties of Eu3+/Sm3+ activated CaZr4(PO4)6 phosphors, J. Fluoresc. 26 (2016) 1865–1873, https://doi.org/10.1007/s10895-016-1880-6.

[19] P. Niu, X. Liu, Y. Wang, W. Zhao, Photoluminescence properties of a novel red-emitting phosphor Ba2LaV3O11:Eu3+, J. Mater. Sci. Mater. Electron. 29 (2018) 124–129, https://doi.org/10.1007/s10854-017-7895-1.

[20] J. Zhao, H. Gao, H. Xu, Z. Zhao, H. Bu, X. Cao, L. He, Z. Yang, J. Sun, Structure and photoluminescence of Eu3+doped Sr2InTaO6red phosphor with high color purity, RSC Adv. 11 (2021) 8282–8289, https://doi.org/10.1039/d1ra00165e.

[21] R. Zhu, Z. Bi, K. Jia, Y. Liu, Y. Lyu, Elucidating the electronic structures and photoluminescence properties of single-phase ScF3:Dy3+, Eu3+, Ce3+ phosphors for LEDs, J. Sol. Gel Sci. Technol. 96 (2020) 753–762, https://doi.org/10.1007/s10971-020-05411-y.

[22] F. Chen, M.N. Akram, X. Chen, Nanocomposite phosphor materials fabricated by solid-state reaction for optoelectronics application, in: Proc. - 2020 IEEE 8th

Electron. Syst. Technol. Conf. ESTC 2020, 2020, pp. 4–7, https://doi.org/10.1109/ESTC48849.2020.9229683.
[23] Y. Wang, B. Zhao, B. Deng, S. Chen, Y. Liu, G. Wang, R. Yu, Spectral properties and Judd−Ofelt analysis of novel red phosphors Gd2InSbO7:Eu3+ with high color purity for white LEDs, J. Rare Earths (2020), https://doi.org/10.1016/j.jre.2020.08.002.
[24] K. Singh, S. Vaidyanathan, Novel narrow band red emitters based on mixed metal oxides and their application in hybrid white light-emitting diodes, Luminescence (2020) 1–12, https://doi.org/10.1002/bio.3975.
[25] M. Sun, Y. Yin, C. Song, Y. Wang, J. Xiao, S. Qu, W. Zheng, C. Li, W. Dong, L. Zhang, Preparation of Bi2MoO6 nanomaterials and theirs gas-sensing properties, J. Inorg. Organomet. Polym. Mater. 26 (2016) 294–301, https://doi.org/10.1007/s10904-015-0316-0.
[26] J. Sottmann, M. Herrmann, P. Vajeeston, A. Ruud, C. Drathen, H. Emerich, D. S. Wragg, H. Fjellvåg, Bismuth vanadate and molybdate: stable Alloying anodes for sodium-ion batteries, Chem. Mater. 29 (2017) 2803–2810, https://doi.org/10.1021/acs.chemmater.6b04699.
[27] K. Lai, W. Wei, Y. Dai, Z. Ruiqin, B. Huang, DFT calculations on structural and electronic properties of Bi 2MO 6 (M = Cr, Mo, W), Rare Met. 30 (2011) 166–172, https://doi.org/10.1007/s12598-011-0262-0.
[28] P. Bégué, J.M. Rojo, J.E. Iglesias, A. Castro, Different [Bi12O14]n columnar structural types in the Bi-Mo-Cr-O system: synthesis, structure, and electrical properties of the solid solution Bi26Mo10-xCrxO69, J. Solid State Chem. 166 (2002) 7–14, https://doi.org/10.1006/jssc.2002.9543.
[29] D. Tang, O. Mabayoje, Y. Lai, Y. Liu, C.B. Mullins, Enhanced photoelectrochemical performance of porous Bi 2 MoO 6 photoanode by an electrochemical treatment, J. Electrochem. Soc. 164 (2017) H299–H306, https://doi.org/10.1149/2.0271706jes.
[30] F. Guo, M. Zhao, K. Xu, Y. Huan, S. Ge, Y. Chen, J. Huang, Y. Cui, J. Zhuang, Y. Du, H. Feng, W. Hao, Evidence for dynamic relaxation behavior of oxygen vacancy in Aurivillius Bi2MoO6 from dielectric spectroscopy during resistance switching, J. Mater. Chem. C. 7 (2019) 8915–8922, https://doi.org/10.1039/c9tc02693b.
[31] J. Zhang, T. Wang, X. Chang, A. Li, J. Gong, Fabrication of porous nanoflake BiMOX (M = W, V, and Mo) photoanodes via hydrothermal anion exchange, Chem. Sci. 7 (2016) 6381–6386, https://doi.org/10.1039/c6sc01803c.
[32] X.-B. Zhang, L. Zhang, J.-S. Hu, X.-H. Huang, Facile hydrothermal synthesis and improved photocatalytic activities of Zn^{2+} doped Bi_2MoO_6 nanosheets, RSC Adv. 6 (2016) 32349–32357, https://doi.org/10.1039/C6RA06972J.
[33] X. Meng, Z. Zhang, Pd-doped Bi2MoO6 plasmonic photocatalysts with enhanced visible light photocatalytic performance, Appl. Surf. Sci. 392 (2017) 169–180, https://doi.org/10.1016/j.apsusc.2016.08.113.
[34] M. Imani, M. Farajnezhad, A. Tadjarodi, 3D hierarchical flower-like nanostructure of Bi2MoO6: mechanochemical synthesis, the effect of synthesis parameters and photocatalytic activity, Mater. Res. Bull. 87 (2017) 92–101, https://doi.org/10.1016/j.materresbull.2016.11.021.
[35] R.B. Licht, A.T. Bell, A DFT investigation of the mechanism of propene ammoxidation over α-bismuth molybdate, ACS Catal. 7 (2017) 161–176, https://doi.org/10.1021/acscatal.6b02523.
[36] S. Sun, W. Wang, Advanced chemical compositions and nanoarchitectures of bismuth based complex oxides for solar photocatalytic application, RSC Adv. 4 (2014) 47136–47152, https://doi.org/10.1039/c4ra06419d.
[37] X. Meng, Z. Zhang, Bismuth-based photocatalytic semiconductors: introduction, challenges and possible approaches, J. Mol. Catal. Chem. 423 (2016) 533–549, https://doi.org/10.1016/j.molcata.2016.07.030.
[38] R. Rangel, G. Díaz, S. Fuentes, D.H. Galván, Comparison between G-Bi2MoO6 and Bi2WO6 Catalysts in the CO Oxidation, vol. 9, 2002, pp. 2–7, https://doi.org/10.1023/A:1014055003830.
[39] M. Ratova, P.J. Kelly, G.T. West, X. Xia, Y. Gao, Deposition of visible light active photocatalytic bismuth molybdate thin films by reactive magnetron sputtering, Materials (Basel) 9 (2016), https://doi.org/10.3390/ma9020067.
[40] J. Xiong, P. Song, J. Di, H. Li, Z. Liu, Freestanding ultrathin bismuth-based materials for diversified photocatalytic applications, J. Mater. Chem. A. 7 (2019) 25203–25226, https://doi.org/10.1039/c9ta10144f.
[41] Q. He, Y. Ni, S. Ye, Heterostructured Bi2O3/Bi2MoO6 nanocomposites: simple construction and enhanced visible-light photocatalytic performance, RSC Adv. 7 (2017) 27089–27099, https://doi.org/10.1039/c7ra02760e.
[42] Y. Hao, X. Dong, S. Zhai, H. Ma, X. Wang, X. Zhang, Hydrogenated bismuth molybdate nanoframe for efficient sunlight-driven nitrogen fixation from air, Chem. Eur J. 22 (2016) 18722–18728, https://doi.org/10.1002/chem.201604510.
[43] S. Wang, X. Ding, X. Zhang, H. Pang, X. Hai, G. Zhan, W. Zhou, H. Song, L. Zhang, H. Chen, J. Ye, In situ carbon homogeneous doping on ultrathin bismuth molybdate: a dual-purpose strategy for efficient molecular oxygen activation, Adv. Funct. Mater. 27 (2017) 1–10, https://doi.org/10.1002/adfm.201703923.
[44] Y. Sen Xu, W. De Zhang, Monodispersed Ag3PO4 nanocrystals loaded on the surface of spherical Bi2MoO6 with enhanced photocatalytic performance, Dalton Trans. 42 (2013) 1094–1101, https://doi.org/10.1039/c2dt31634j.
[45] J.J. Mu, G.H. Zheng, Y.Q. Ma, Morphology and photocatalytic properties of γ-Bi2MoO6 tuned by stirring and surfactant EDTA assistant, J. Electron. Mater. 46 (2017) 596–601, https://doi.org/10.1007/s11664-016-4925-3.
[46] Y.N. Zhu, J.J. Mu, G.H. Zheng, Z.X. Dai, L.Y. Zhang, Y.Q. Ma, D.W. Zhang, Morphology, photocatalytic and photoelectric properties of Bi2MoO6 tuned by preparation method, solvent, and surfactant, Ceram. Int. 42 (2016) 17347–17356, https://doi.org/10.1016/j.ceramint.2016.08.031.
[47] M. Jin, S. Lu, L. Ma, M. Gan, One-step synthesis of in situ reduced metal Bi decorated bismuth molybdate hollow microspheres with enhancing photocatalytic activity, Appl. Surf. Sci. 396 (2017) 438–443, https://doi.org/10.1016/j.apsusc.2016.10.173.
[48] E. Hong, J.H. Park, C.H. Shin, Oxidative dehydrogenation of n-butenes to 1,3-butadiene over bismuth molybdate and ferrite catalysts: a review, Catal. Surv. Asia 20 (2016) 23–33, https://doi.org/10.1007/s10563-015-9201-7.
[49] Q. He, Y. Ni, S. Ye, Preparation of flowerlike BiOBr/Bi2MoO6 composite superstructures and the adsorption behavior to dyes, J. Phys. Chem. Solid. 104 (2017) 286–292, https://doi.org/10.1016/j.jpcs.2017.01.020.
[50] H. Li, T. Hu, R. Zhang, J. Liu, W. Hou, Preparation of solid-state Z-scheme Bi2MoO6/MO (MCu, Co3/4, or Ni) heterojunctions with internal electric field-improved performance in photocatalysis, Appl. Catal. B Environ. 188 (2016) 313–323, https://doi.org/10.1016/j.apcatb.2016.02.015.
[51] X. Ding, W. Ho, J. Shang, L. Zhang, Self doping promoted photocatalytic removal of no under visible light with bi2moo6: indispensable role of superoxide ions, Appl. Catal. B Environ. 182 (2016) 316–325, https://doi.org/10.1016/j.apcatb.2015.09.046.
[52] M. Wu, Y. Wang, Y. Xu, J. Ming, M. Zhou, R. Xu, Q. Fu, Y. Lei, Self-supported Bi 2 MoO 6 nanowall for photoelectrochemical water splitting, ACS Appl. Mater. Interfaces 9 (2017) 23647–23653, https://doi.org/10.1021/acsami.7b03801.
[53] Y. Peng, Y. Zhang, F. Tian, J. Zhang, J. Yu, Structure tuning of Bi 2 MoO 6 and their enhanced visible light photocatalytic performances, Crit. Rev. Solid State Mater. Sci. 42 (2017) 347–372, https://doi.org/10.1080/10408436.2016.1200009.
[54] M.T. Le, V.H. Do, D.D. Truong, E. Bruneel, I. Van Driessche, A. Riisager, R. Fehrmann, Q.T. Trinh, Synergy effects of the mixture of bismuth molybdate catalysts with SnO2/ZrO2/MgO in selective propene oxidation and the connection between conductivity and catalytic activity, Ind. Eng. Chem. Res. 55 (2016) 4846–4855, https://doi.org/10.1021/acs.iecr.6b00019.
[55] W.J.M. van Well, M.T. Le, N.C. Schiødt, S. Hoste, P. Stoltze, The influence of the calcination conditions on the catalytic activity of Bi2MoO6 in the selective oxidation of propylene to acrolein, J. Mol. Catal. Chem. 256 (2006) 1–8, https://doi.org/10.1016/j.molcata.2006.04.030.
[56] L. Zhou, W. Wang, L. Zhang, Ultrasonic-assisted synthesis of visible-light-induced Bi2MO6 (M = W, Mo) photocatalysts, J. Mol. Catal. Chem. 268 (2007) 195–200, https://doi.org/10.1016/j.molcata.2006.12.026.
[57] T. Chen, M.H. Wang, X.Y. Ma, Preparation in acidic and alkaline conditions and characterization of α-Bi 2 Mo 3 O 12 and γ-Bi 2 MoO 6 powders, J. Electron. Mater. 45 (2016) 4375–4379, https://doi.org/10.1007/s11664-016-4648-5.
[58] D.P. Dutta, A. Ballal, S. Chopade, A. Kumar, A study on the effect of transition metal (Ti4+, Mn2+, Cu2+ and Zn2+)-doping on visible light photocatalytic activity of Bi2MoO6 nanorods, J. Photochem. Photobiol. Chem. 346 (2017) 105–112, https://doi.org/10.1016/j.jphotochem.2017.05.044.
[59] B. Han, B. Liu, J. Zhang, P. Li, H. Shi, Comparative photoluminescence properties and Judd–Ofelt analysis of Eu3+ ion-activated metal molybdate phosphors A2MoO6:Eu3+ (A = La, Y, Gd and Bi), J. Electron. Mater. 46 (2017) 4039–4046, https://doi.org/10.1007/s11664-017-5390-3.
[60] Z. Dai, F. Qin, H. Zhao, J. Ding, Y. Liu, R. Chen, Crystal defect engineering of aurivillius Bi 2 MoO 6 by Ce doping for increased reactive species production in photocatalysis, ACS Catal. 6 (2016) 3180–3192, https://doi.org/10.1021/acscatal.6b00490.
[61] H. Li, W. Li, S. Gu, F. Wang, H. Zhou, X. Liu, C. Ren, Enhancement of photocatalytic activity in Tb/Eu co-doped Bi2MoO6: the synergistic effect of Tb-Eu redox cycles, RSC Adv. 6 (2016) 48089–48098, https://doi.org/10.1039/c6ra08739f.
[62] H. Li, W. Li, F. Wang, X. Liu, C. Ren, Fabrication of two lanthanides co-doped Bi2MoO6photocatalyst: selection, design and mechanism of Ln1/Ln2redox couple for enhancing photocatalytic activity, Appl. Catal. B Environ. 217 (2017) 378–387, https://doi.org/10.1016/j.apcatb.2017.06.015.
[63] M. Guan, X. He, T. Shang, J. Sun, Q. Zhou, Hydrothermal synthesis of ultrathin Bi2MO6 (M=W, Mo) nanoplates as new host substances for red-emitting europium ion, Prog. Nat. Sci. Mater. Int. 22 (2012) 334–340, https://doi.org/10.1016/j.pnsc.2012.09.002.
[64] Z.J. Zhang, X.Y. Chen, Sb2MoO6, Bi2MoO6, Sb2WO6, and Bi2WO6 flake-like crystals: generalized hydrothermal synthesis and the applications of Bi2WO6 and Bi2MoO6 as red phosphors doped with Eu3+ ions, Mater. Sci. Eng. B Solid-State Mater. Adv. Technol. 209 (2016) 10–16, https://doi.org/10.1016/j.mseb.2015.12.003.
[65] M. Maçzka, W. Paraguassu, L. Macalik, P.T.C. Freire, J. Hanuza, J. Mendes Filho, A Raman scattering study of pressure-induced phase transitions in nanocrystalline Bi2MoO6, J. Phys. Condens. Matter 23 (2011), https://doi.org/10.1088/0953-8984/23/4/045401.
[66] X. Wu, Y.H. Ng, W.H. Saputera, X. Wen, Y. Du, S.X. Dou, R. Amal, J. Scott, The dependence of Bi2MoO6 photocatalytic water oxidation capability on crystal facet engineering, ChemPhotoChem 3 (2019) 1246–1253, https://doi.org/10.1002/cptc.201900113.
[67] A.A. Alemi, R. Kashfi, B. Shabani, Preparation and characterization of novel Ln (Gd3+, Ho 3+ and Yb3+)-doped Bi2MoO6 with Aurivillius layered structures and photocatalytic activities under visible light irradiation, J. Mol. Catal. Chem. 392 (2014) 290–298, https://doi.org/10.1016/j.molcata.2014.05.029.
[68] M. Wang, P. Guo, G. Yang, T. Chai, T. Zhu, The honeycomb-like Eu3+, Fe3+ doping bismuth molybdate photocatalyst with enhanced performance prepared by a citric acid complex process, Mater. Lett. 192 (2017) 96–100, https://doi.org/10.1016/j.matlet.2016.12.050.
[69] L. Xie, J. Ma, G. Xu, Preparation of a novel Bi2MoO6 flake-like nanophotocatalyst by molten salt method and evaluation for photocatalytic decomposition of rhodamine B, Mater. Chem. Phys. 110 (2008) 197–200, https://doi.org/10.1016/j.matchemphys.2008.01.035.

[70] K.V. Terebilenko, Effect of structure on the luminescent characteristics of complex oxide compounds of bismuth(III) doped with europium(III), Theor. Exp. Chem. 50 (2015) 352–357, https://doi.org/10.1007/s11237-015-9387-9.
[71] P. Dumrongrojthanath, T. Thongtem, A. Phuruangrat, S. Thongtem, Glycothermal synthesis of Dy-doped Bi2MoO6 nanoplates and their photocatalytic performance, Res. Chem. Intermed. 42 (2016) 5087–5097, https://doi.org/10.1007/s11164-015-2346-1.
[72] D. Liang, Y. Ding, N. Wang, X. Cai, J. Li, L. Han, S. Wang, Y. Han, G. Jia, L. Wang, Solid-state reaction synthesis for mixed-phase Eu3+-doped bismuth molybdate and its luminescence properties, Mod. Phys. Lett. B 31 (2017) 1750241, https://doi.org/10.1142/s0217984917502414.
[73] X.H. He, M.Y. Guan, J.H. Sun, N. Lian, T.M. Shang, Synthesis and photoluminescence properties of LiEu(W,Mo)2O 8:Bi3+ red-emitting phosphor for white-LEDs, J. Mater. Sci. 45 (2010) 118–123, https://doi.org/10.1007/s10853-009-3900-2.
[74] R. Kashfi-Sadabad, S. Yazdani, A. Alemi, T.D. Huan, R. Ramprasad, M.T. Pettes, Block copolymer-assisted solvothermal synthesis of hollow Bi2MoO6 spheres substituted with samarium, Langmuir 32 (2016) 10967–10976, https://doi.org/10.1021/acs.langmuir.6b02854.
[75] I.M. Pinatti, T.G. Ireland, G.R. Fern, I.L.V. Rosa, J. Silver, Low temperature micro Raman and laser induced upconversion and downconversion spectra of europium doped silver tungstate Ag2−3xEuxWO4 nanorods, J. Mater. Sci. Mater. Electron. 28 (2017) 7029–7035, https://doi.org/10.1007/s10854-016-6077-x.
[76] I.M. Pinatti, G.R. Fern, E. Longo, T.G. Ireland, P.F.S. Pereira, I.L.V. Rosa, J. Silver, Luminescence properties of α-Ag2WO4 nanorods co-doped with Li+ and Eu3+ cations and their effects on its structure, J. Lumin. 206 (2019) 442–454, https://doi.org/10.1016/j.jlumin.2018.10.104.
[77] I.M. Pinatti, I.C. Nogueira, W.S. Pereira, P.F.S. Pereira, R.F. Gonçalves, J.A. Varela, E. Longo, I.L.V. Rosa, Structural and photoluminescence properties of Eu3+ doped α-Ag2WO4 synthesized by the green coprecipitation methodology, Dalton Trans. 44 (2015) 17673–17685, https://doi.org/10.1039/c5dt01997d.
[78] L.X. Lovisa, J. Andrés, L. Gracia, M.S. Li, C.A. Paskocimas, M.R.D. Bomio, V. D. Araujo, E. Longo, F.V. Motta, Photoluminescent properties of ZrO2: Tm3+, Tb3+, Eu3+powders—a combined experimental and theoretical study, J. Alloys Compd. 695 (2017) 3094–3103, https://doi.org/10.1016/j.jallcom.2016.11.341.
[79] I.L.V. Rosa, F.A. Tavares, A.P. de Moura, I.M. Pinatti, L.F. da Silva, M.S. Li, E. Longo, Luminescent and gas sensor properties of the ZrO2:Hhpa:Eu3+ hybrid compound, J. Lumin. 197 (2018) 38–46, https://doi.org/10.1016/j.jlumin.2017.12.046.
[80] R.L. Tranquilin, L.X. Lovisa, C.R.R. Almeida, C.A. Paskocimas, M.S. Li, M. C. Oliveira, L. Gracia, J. Andres, E. Longo, F.V. Motta, M.R.D. Bomio, Understanding the white-emitting CaMoO4 Co-doped Eu3+, Tb3+, and Tm3+ phosphor through experiment and computation, J. Phys. Chem. C 123 (2019) 18536–18550, https://doi.org/10.1021/acs.jpcc.9b04123.
[81] L.X. Lovisa, M.C. Oliveira, J. Andrés, L. Gracia, M.S. Li, E. Longo, R.L. Tranquilin, C.A. Paskocimas, M.R.D. Bomio, F.V. Motta, Structure, morphology and photoluminescence emissions of ZnMoO4: RE 3+=Tb3+ - Tm3+ - X Eu3+ (x = 1, 1.5, 2, 2.5 and 3 mol%) particles obtained by the sonochemical method, J. Alloys Compd. 750 (2018) 55–70, https://doi.org/10.1016/j.jallcom.2018.03.394.
[82] M.C. Oliveira, R.A.P. Ribeiro, L. Gracia, S.R. De Lazaro, M. De Assis, M. Oliva, I.L. V. Rosa, M.F.D.C. Gurgel, E. Longo, J. Andrés, Experimental and theoretical study of the energetic, morphological, and photoluminescence properties of CaZrO3:Eu3+, CrystEngComm 20 (2018) 5519–5530, https://doi.org/10.1039/c8ce00964c.
[83] L. Feng, M. Li, K. Pan, R. Li, N. Fan, G. Wang, Photoluminescence and photocatalytic activity of Bi2MoO6:Ln3+ nanocrystals, J. Nanosci. Nanotechnol. 16 (2016) 3781–3785, https://doi.org/10.1166/jnn.2016.11850.
[84] J. Zhang, Y. Liu, L. Li, N. Zhang, L. Zou, S. Gan, Hydrothermal synthesis, characterization, and color-tunable luminescence properties of Bi2MoO6:Eu3+ phosphors, RSC Adv. 5 (2015) 29346–29352, https://doi.org/10.1039/c5ra03913d.
[85] B.N. Naidu, K.K. Rao, M.P.S. Murali Krishna, Semi sol-gel synthesis and red luminescence studies of Eu 3+ activated Double perovskite phosphors Bi 2-x Eu x MoO 6 (x=0.0–0.24), Optik (Stuttg) 182 (2019) 565–570, https://doi.org/10.1016/j.ijleo.2019.01.086.
[86] X. Jiang, S. Song, J. Guo, W. Lv, Y. Li, X. Guo, X. Wang, H. Liu, Y. Han, L. Wang, Solid-state synthesis and fluorescence properties of micron Bi2MoO6:Eu3+/C3N4 composite phosphors, Phys. Lett. Sect. A Gen. At. Solid State Phys. 384 (2020) 126149, https://doi.org/10.1016/j.physleta.2019.126149.
[87] J. Huang, J. Loriers, P. Porcher, Spectroscopic properties of some Eu3+ doped scheelite-related rare earth sesquimolybdates and sesquitungstates, J. Solid State Chem. 48 (1983) 333–345, https://doi.org/10.1016/0022-4596(83)90090-7.
[88] B. Han, J. Zhang, P. Li, J. Li, Y. Bian, H. Shi, Synthesis and luminescence properties of Eu3+ doped high temperature form of BiMoO6, J. Electron. Mater. 44 (2015) 1028–1033, https://doi.org/10.1007/s11664-014-3621-4.
[89] A.W. Hewat, A. Laarif, The structure of koechlinite bismuth molybdate-A controversy resolved by neutron diffraction, Ferroelectrics 56 (1984) 219–237, https://doi.org/10.1080/00150198408221372.
[90] K. Momma, F. Izumi, VESTA 3 for three-dimensional visualization of crystal, volumetric and morphology data, J. Appl. Crystallogr. 44 (2011) 1272–1276, https://doi.org/10.1107/S0021889811038970.
[91] K. Momma, F. Izumi, VESTA : a three-dimensional visualization system for electronic and structural analysis, J. Appl. Crystallogr. 41 (2008) 653–658, https://doi.org/10.1107/s0021889808012016.
[92] R.D. Shannon, Revised effective ionic radii in halides and chalcogenides, Acta Crystallogr. (1976) 751, https://doi.org/10.1107/S0567739476001551.
[93] Y. Chen, Y. Lan, D. Wang, G. Zhang, W. Peng, Y. Chen, Q. Zeng, X. He, J. Wang, Luminescent properties of Gd2MoO6:Eu3+ nanophosphor for WLEDs, Dalton Trans. (2021) 6281–6289, https://doi.org/10.1039/d1dt00547b.
[94] X. Liu, W. Zhou, F. Li, C. Yu, Eu3+ doped Bi2MoO6 nanosheets fabricated via hydrothermal-calcination route and their superior performance for aqueous volatile phenols removal, J. Taiwan Inst. Chem. Eng. 125 (2021) 276–284, https://doi.org/10.1016/j.jtice.2021.06.038.
[95] P.B. Almeida, I.M. Pinatti, R.C. de Oliveira, M.M. Teixeira, C.C. Santos, T. R. Machado, E. Longo, I.L.V. Rosa, Structural, morphological and photoluminescence properties of β-Ag2MoO4 doped with Eu3+, Chem. Pap. (2021) https://doi.org/10.1007/s11696-020-01489-4.
[96] M. Maęzka, L. Macalik, K. Hermanowicz, L. Kępiński, J. Hanuza, Synthesis and phonon properties of nanosized aurivillius phase of Bi 2MoO6, J. Raman Spectrosc. 41 (2010) 1289–1296, https://doi.org/10.1002/jrs.2568.